PHYSICS OF FLUIDS **24**, 126601 (2012)

The generation of zonal jets by large-scale mixing

R. K. Scott[1,2] and A.-S. Tissier[3]
[1]*School of Mathematics, University of St Andrews, St Andrews KY16 9SS, Scotland*
[2]*Northwest Research Associates, Seattle, Washington 98052, USA*
[3]*Laboratoire de Météorologie Dynamique, UMR8539, UPMC/ENS/CNRS/Ecole Polytechnique, Paris, France*

(Received 1 June 2012; accepted 6 November 2012; published online 19 December 2012)

The development of zonal flows on a midlatitude β-plane subject to a time-varying topographic forcing is investigated in a series of numerical integrations in which the forcing is concentrated at large scales, and in which the usual two-dimensional inverse energy cascade is absent. In contrast to the case of small-scale forcing, where mixing of potential vorticity occurs largely through the action of small-scale eddies, mixing of potential vorticity in this case occurs predominantly in latitudinally localized Rossby wave critical layer regions, whose width grows continuously in time due to the entrainment of background fluid. The potential vorticity is found to organize into a piecewise constant staircase-like profile, monotonic in latitude, provided the ratio $L_{\mathrm{Rh}}/L_f \gtrsim 1$, where L_{Rh} is the usual Rhines scale and L_f is the scale of the forcing; this may be regarded as supplemental to the condition $L_{\mathrm{Rh}}/L_\varepsilon \gtrsim 6$, where $L_\varepsilon = (\varepsilon/\beta^3)^{1/5}$ and ε is the rate of energy input, obtained recently [R. K. Scott and D. G. Dritschel, "The structure of zonal jets in geostrophic turbulence," J. Fluid Mech. **711**, 576–598 (2012)] for the case of small-scale forcing. The numerical results further suggest that the nature of the potential vorticity mixing is controlled by the ratio L_ε/L_f, and occurs predominantly in critical layers when $L_\varepsilon/L_f \lesssim 1/6$. A combined condition for staircase formation may therefore be expressed as $L_{\mathrm{Rh}}/L_\varepsilon \gtrsim \max\{6, L_f/L_\varepsilon\}$. Finally, in a separate set of experiments it is shown that when forcing is represented by an additive source term in the evolution equation, as is common practice in numerical investigations of two-dimensional turbulence, the effect of non-conservation of potential vorticity may obscure the development of the staircase profile in the critical layer mixing dominated regime. © *2012 American Institute of Physics*. [http://dx.doi.org/10.1063/1.4771991]

I. INTRODUCTION

A striking feature of the large-scale turbulent motions of atmospheres and oceans, influenced by the constraining effects of rapid rotation and stable stratification, is the presence of well-defined zonal, or longitudinally aligned, jets coexisting with a background turbulent flow. Different explanations have been put forward for the emergence of zonal flows but all are linked to the natural tendency for eddy and Rossby wave motions to mix potential vorticity, a quantity comprising in the simplest case the relative vorticity plus a component due to the planetary rotation, whose background gradient also provides the restoring force for the Rossby waves themselves. Through the anisotropy of the background gradient, generation and dissipation of these waves give rise directly to accelerations in the zonal direction, the eddy fluxes of potential vorticity being related to the convergence of the eddy flux of zonal momentum through a generalized Taylor identity.[1–4] Eddy mixing of potential vorticity may be used as a general framework to describe jet formation in many situations, including those where eddies arise internally from instability of a basic state of non-trivial vertical structure, where now the location of mixing zones may depend on their relation to the underlying baroclinicity.[5] In such situations, complete understanding of the details of the jet development may require separate

consideration of momentum flux convergences associated with barotropic and baroclinic components of the flow.[6]

The traditional explanation for the emergence of zonal jets has been given less often in term of the actual mechanisms through which Rossby waves mix potential vorticity, but more usually in terms of the phenomenological description of two-dimensional turbulence. In a forced two-dimensional flow in which eddies are generated at small scales, the inverse energy cascade results in an increase over time of typical eddy length scales, L, and a corresponding increase in the eddy timescale $\tau \sim L/U$, where U is a typical eddy velocity. The Rhines scale[7,8] $L_{\mathrm{Rh}} = \sqrt{U/\beta}$ may be considered as the scale at which the eddy timescale τ becomes comparable with the timescale for Rossby wave motions $\tau_R \sim 1/\beta L$ (the latter being typically longer than the timescale for smaller eddies). Because transience or dissipation of Rossby waves may induce zonal accelerations, at the simplest level, the Rhines scale describes the scale at which waves and zonal motions may become important (although some care is needed in the interpretation of U of in the definition of L_{Rh}; see, e.g., the discussion in Ref. 9). In certain cases, in which the potential vorticity is perfectly mixed in latitudinal zones between strong jets and develops a monotonic, piecewise constant, staircase-like distribution in latitude, the Rhines scale can be shown to vary directly with the (half) spacing between jets, L_j, as $L_j = \sqrt{3}L_{\mathrm{Rh}}$, where the U in L_{Rh} is taken as the maximum (eastward) jet velocity.[4,10]

The staircase limit itself can be achieved provided the small-scale forcing is weak enough that turbulent eddy intensities are smaller than the jump in potential vorticity across the jets. This was made precise in Ref. 9, where it was demonstrated that the staircase limit is approached when the parameter $L_{\mathrm{Rh}}/L_\varepsilon$ becomes sufficiently large (in the range 6–10); here $L_\varepsilon = (\varepsilon/\beta^3)^{1/5}$, where ε is the rate of energy input, or energy flux to large scales, as first introduced by Maltrud and Vallis.[11] (The parameter $L_{\mathrm{Rh}}/L_\varepsilon$ was also discussed recently in relation to the frictional halting of the inverse cascade.[12,13]) For smaller values of $L_{\mathrm{Rh}}/L_\varepsilon$, for which the energy input rate is larger (for given L_{Rh}), eddy intensities are large enough to continually disrupt the potential vorticity gradients in jet cores and keep the zonal average potential vorticity gradients close to the background value β.

Although the halting of the inverse cascade by the generation of wave motions is often cited as the mechanism responsible for the emergence of zonal jets in geostrophic turbulent flows,[7,11,13–16] it has long been recognized that more general mixing of potential vorticity also gives rise to zonal accelerations. McIntyre[17] described the intensification of the stratospheric polar night jet in terms of the mixing of potential vorticity in a wide surf zone surrounding the jet, essentially a Rossby wave critical layer, by the action of breaking planetary-scale Rossby waves propagating upwards from lower altitudes. The mixing of potential vorticity in the surf zone is accompanied by a steepening of potential vorticity gradients at the surf zone edge and an intensification of the jet.[18,19] The potential vorticity itself is again mixed into a staircase-like profile.

This scenario suggests that jet formation may be considered completely independently from dynamical processes associated with the two-dimensional turbulent inverse cascade, at least for the case (as in the winter stratosphere) where the large-scale radiative forcing is towards a state of quasi-uniform background shear, on which critical layer mixing of potential vorticity may take place. In this paper, we consider the more general problem in which there is no pre-existing background shear (or large-scale radiative forcing) and consider whether critical layer mixing and associated jet formation may develop spontaneously from purely isotropic large-scale wave forcing and when no inverse cascade is present. In particular, we consider the conditions under which such critical layer mixing may give rise to strong zonal jets that exhibit a monotonic, piecewise constant staircase-like distribution, with jumps in potential vorticity in the jet cores and uniform mixed zones in between. Our results also demonstrate important differences between mixing of potential vorticity by small-scale eddies and by large-scale wave breaking.

In Ref. 9, the forcing was considered to be at scales sufficiently small compared with L_{Rh} that the actual forcing scale was not important (this was supported by the comparison of different forcing mechanisms, with different power spectra, considered in that paper). When the forcing scale L_f is large or comparable to the scales L_{Rh} and L_ε, it may not be ignored in this way and the relative sizes of the three length scales must be considered. The way in which this is achieved in the present paper is described next in Sec. II, together with details of the formulation of the numerical experiments. The main results are then presented in Sec. III with a characterization of the distinct mixing regimes

given in Sec IV. In Sec. V, a short discussion of an alternative forcing method is presented, one commonly used in studies of two-dimensional turbulence because of the convenience in which the energy input rate may be prescribed, but which turns out to be ill-suited to the present problem due to its non-conservative nature. The results are summarized briefly in Sec. VI.

II. TOPOGRAPHIC FORCING

We consider the two-dimensional barotropic quasigeostrophic equations on a mid-latitude β-plane, forced by time-varying bottom topography of random spatial and temporal dependence as further described below. The evolution is specified by exact material advection of potential vorticity, q,

$$q_t + J(\psi, q) = 0, \tag{1}$$

where J is the Jacobean determinant. The advecting flow is determined by the streamfunction ψ which is related to q through

$$q = \beta y + \nabla^2 \psi + q_{\text{topo}}, \tag{2}$$

where the term $q_{\text{topo}} = q_{\text{topo}}(x, y, t)$ represents the topographic forcing, concentrated at some scale L_f, where the effects of varying layer depth are equivalent to the potential vorticity anomaly q_{topo}. The form of forcing has a long history in studies of geophysical fluid dynamics, and is a natural choice for many situations of interest in the present context, such as the winter stratosphere, where q_{topo} may be thought of as a simple representation of the effects of an undulating tropopause. Time-varying topography was suggested by McIntyre[3] as a suitable forcing mechanism relevant for the case of atmospheric and oceanic jets: specifically, it has the advantage that it does not break the material conservation of potential vorticity, and so the Taylor identity provides a meaningful indication of zonal accelerations arising from potential vorticity fluxes.

Equation (1) is solved in a doubly periodic domain. Length and time are scaled such that the domain length is 2π in each direction and $\beta = 1$. We use a standard pseudo-spectral algorithm with a spectral filter[20] in place of the traditional two-thirds dealiasing, and a small-scale hyperviscosity of the form $\nu\nabla^8 q$ as a numerical means of controlling the enstrophy build-up at small scales (with no intended physical interpretation). The time integration is a fourth-order Runge-Kutta scheme. The grid resolution is a modest 512×512, to facilitate very long integrations, and is sufficient to represent the mixing due to the large-scale forcing (selected integrations carried out at half or double this resolution produced no qualitative difference in the results). In the weakest forcing case the integration is continued to $T = 640\,000$. In general the integration length is set to $T = 640/a_0$ where a_0 is a measure of the root mean square topographic forcing amplitude, as defined below, taking values from 0.001 to 0.128 in factors of 2.

Although common in the geophysical context, the form of forcing described above has been less widely used in studies of isotropic two-dimensional turbulence, in which numerical investigations more typically use an additive forcing of the form

$$q_t + J(\psi, q) = F, \tag{3}$$

where now

$$q = \beta y + \nabla^2 \psi \tag{4}$$

and where F is a prescribed, typically random, force on the flow. In part, this choice is made because of the relative ease in which the rate of energy input, ε to the system may be specified, for example, in the case where the forcing is δ-correlated in time, or has a Markovian time-dependence with finite decorrelation timescale. One obvious disadvantage, on the other hand, at least in the present context of a model of geophysical relevance, is that material conservation of potential vorticity is not preserved. Further, in cases where material conservation is strongly violated the relation between eddy potential vorticity fluxes and zonal accelerations is obscured.[3] As discussed further in Sec. IV below, non-conservation of q will become more apparent in cases where the typical forcing scales are large, because the relative magnitude of the advective term $J(\psi, q)$ to the forcing term F will

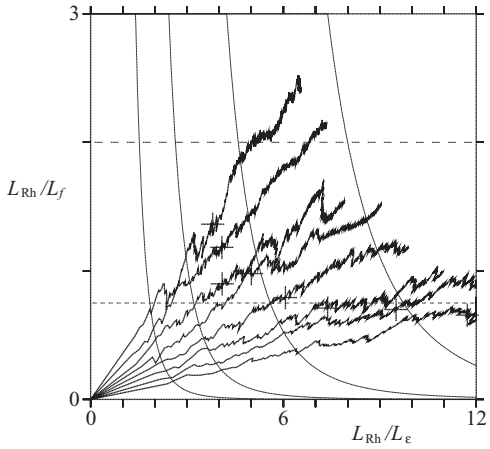

FIG. 1. Energy evolution, L_{Rh}/L_f against $L_{\mathrm{Rh}}/L_\varepsilon$ for cases with $k_f = 2$ and topographic forcing amplitude $a_0 = 0.001$, 0.002, 0.004, 0.008, 0.016, 0.032, 0.064, 0.128. Crosses indicate the first occurrence of $\min(dq/dy_e) < 0.1$; see text for details.

tend to be small. In the current paper, where the focus is on the effect of large-scale forcing on the advective mixing of potential vorticity, it is more desirable to use the conservative topographic forcing and eliminate any issue of non-conservation at the outset, at the expense of some difficulty in constraining precisely the rate of energy input.

A related issue concerns the equilibration of the flow. In studies of isotropic turbulence with small-scale forcing, a frictional term $-rq$ is often added to the right-hand side of (3) to balance energy input by its removal at large scales and to allow a statistically stationary state of fixed energy to be reached. Such a choice is not appropriate to the present situation for two reasons. First, such a non-conservative term again has the undesirable consequence of obscuring the advective mixing of potential vorticity. Second, the frictional term removes energy predominantly at the large scales, precisely at those scales at which the forcing is concentrated in the present situation.

In fact, whether or not the flow reaches a statistically stationary state turns out to be of minor significance in the present situation due to the slow nature of the flow evolution in time. If we assume, initially, a constant rate of energy input by the topographic forcing, and identify the velocity scale U with $U_{\mathrm{rms}} = (2\varepsilon t)^{1/2}$, then the evolution of the Rhines scale follows $L_{\mathrm{Rh}} = \beta^{-1/2}(2\varepsilon t)^{1/4}$. This slow growth in time suggests that the flow will have time to adjust to a state of quasi-equilibrium, except for isolated transitions in the flow in the form of jet mergers associated with increasing L_{Rh} (or, equivalently, the interjet spacing L_j). This has the additional, practical advantage that the two-dimensional parameter space under consideration, spanned, for example, by $L_{\mathrm{Rh}}/L_\varepsilon$ and L_{Rh}/L_f may be investigated with a one-parameter set of numerical integrations of (1), the other dimension being swept out in time during the course of each integration. The situation is illustrated graphically in Fig. 1, each of the bold lines corresponding to a single integration with time increasing from $t = 0$. For comparison, note that the narrow-band integrations carried out in Ref. 9 consist of a series of steady state calculations with values of $L_{\mathrm{Rh}}/L_\varepsilon$ lying along the dashed line at $L_{\mathrm{Rh}}/L_f = 2$. (The broad-band integrations of Ref. 9 have less well-defined L_f, but lie in the region above the dashed line.) Whereas Ref. 9 was concerned with the change in jet structure as $L_{\mathrm{Rh}}/L_\varepsilon$ varied along the dashed line, here we are interested in how this dependence changes at lower values of L_{Rh}/L_f.

At any given time, t, the function q_{topo} is defined via its Fourier transform $\hat{f}_{\mathbf{k}}$, which satisfies $\langle \hat{f}_{\mathbf{k}} \hat{f}^*_{\mathbf{k}} \rangle = F(k)/\pi k$, with spectrum $F(k) = a^2(t)$ for $k \in [k_f - \delta_k, k_f + \delta_k]$ and $F(k) = 0$ otherwise, for some forcing wavenumber $k_f = L_f^{-1}$, where δ_k is a specified bandwidth and $\langle \cdot \rangle$ denotes an ensemble average over all wavenumbers with $|\mathbf{k}| = k$. The function $a(t)$ may be thought of as a mean topographic amplitude, defined below. Here, we use the values $k_f = 2$ and $\delta_k = 1$. It is natural to use a Markovian time-dependence for each Fourier mode $\hat{f}_{\mathbf{k}}$, if we consider the situation in which the topographic forcing represents a dynamic interface such as the tropopause or thermocline, undulating up or down in response to wave motions in the denser lower layer. At time step n, we

thus define an intermediate function

$$\tilde{f}_{\mathbf{k}}^{(n)} = \alpha \tilde{f}_{\mathbf{k}}^{(n-1)} + \sqrt{1-\alpha^2}\sigma_{\mathbf{k}}, \tag{5}$$

where $\sigma_{\mathbf{k}}$ is a random variable of zero mean, uniformly distributed on $[-1, 1]$, and define

$$\hat{f}_{\mathbf{k}}^{(n)} = \frac{a(t)\tilde{f}_{\mathbf{k}}^{(n)}}{\langle \tilde{f}_{\mathbf{k}}^{(n)} \tilde{f}_{\mathbf{k}}^{*(n)} \rangle^{1/2}}, \tag{6}$$

where $\langle \cdot \rangle$ is an average over all wavenumbers, ensuring that the root mean square topography $\langle \hat{f}_{\mathbf{k}}^{(n)} \hat{f}_{\mathbf{k}}^{*(n)} \rangle^{1/2} = a(t)$ at any given time. The parameter α is related to the decorrelation time τ_f via $\alpha = 1 - \Delta t/\tau_f$, where Δt is the time step, so that $\tau_f = \Delta t$ for $\alpha = 0$ (delta-correlated forcing) and $\tau_f = \infty$ for $\alpha = 1$ (steady forcing). A natural choice for τ_f, again considering the situation of a tropopause or thermocline undulating due to wave motions below, is then the inverse Rossby wave frequency for wavenumbers around k_f. This yields a value of $\tau_f = 5/\beta$ for wavenumbers in the range 1–3, which we fix across all integrations. The results, however, are remarkably insensitive to the choice of τ_f. The time dependent forcing amplitude $a(t)$ is defined as

$$a(t) = a_0(1 - e^{-t/\tau_f}) \tag{7}$$

to avoid strong initial transients and to reach an essentially constant value a_0 at early time.

Multiplying (1) by ψ and integrating over the domain yields the energy equation

$$\dot{\mathcal{E}} = \langle \psi \partial_t q_{\text{topo}} \rangle, \tag{8}$$

where $\mathcal{E}$ is the total energy. With τ_f fixed, the rate of energy input depends quadratically on the forcing amplitude a_0 (since the forcing induces $O(a_0)$ changes to ψ) at least initially, before substantial mean flows develop. It should be emphasized, however, that this is only an approximate scaling and that the actual energy input rate at a give time in a given realization depends also on the state of the flow itself; in some cases periods during which the total energy decreases are even observed, corresponding to a negative energy input rate by the forcing. In fact, in the long term, there is a reasonably linear average growth of the energy: the slopes in Fig. 1, indicating L_ε/L_f, are approximately uniform across the full length of each integration. The actual energy growth across all calculations is summarized in Fig. 2, showing $\mathcal{E}/a_0$ against $a_0 t$. The length of each integration is scaled as $1/a_0$ to allow for sufficient energy growth in the weaker forcing cases and to provide a better coverage of the parameter space as shown in Fig. 1 (since the energy input rate scales approximately as a_0^2 this means that the final energy of each case increases approximately as a_0). Figure 2 verifies that on average energy input, rates scale approximately as a_0^2 albeit with a large variance. There is no systematic variation in the

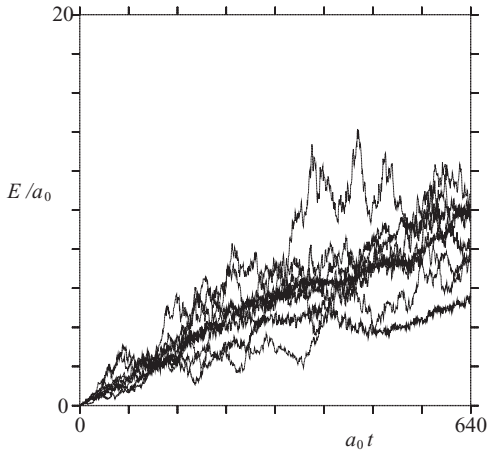

FIG. 2. Scaled energy evolution, E/a_0 against $a_0 t$ for cases with $k_f = 2$ and topographic forcing amplitude $a_0 = 0.001, 0.002, 0.004, 0.008$ (thin lines) and $a_0 = 0.016, 0.032, 0.064, 0.128$ (bold lines).

curves, however, with the four strongest forcing cases (bold) occupying approximately the same range as the four weakest cases (thin).

In addition to the Rossby wave frequency, an enstrophy based timescale may be defined from the energy input rate by $T_\eta = (k_f^2 \varepsilon)^{-1/3}$. In the case in which nonlinear, coherent eddies created by the forcing directly mix potential vorticity, it may be expected that the development of zonal jets might occur on a timescale proportional to T_η, independently of ε and k_f. In the parameter space depicted in Fig. 1, lines of constant t/T_η are given by the curves $(L_{\mathrm{Rh}}/L_f)(L_{\mathrm{Rh}}/L_\varepsilon)^5 = C_T$ = constant, and are indicated by the thin hyperbolic lines (indicating times $t = \frac{1}{2} C_T^{2/3} \beta^{-5/3} T_\eta$ with C_T taking the values 4, 8, 12, 16). In fact, as discussed further below, this timescale fails to predict the development of zonal jets for cases with weaker forcing, in which jets first develop typically when the energy reaches a level such that the ratio L_{Rh}/L_f exceeds a value of around $\frac{3}{4}$ (dotted line in Fig. 1; based on a measure of the potential vorticity gradients, described further below, the onset of jet development in each integration is indicated by a cross mark). The reason for the failure of T_η in these cases appears to be due to the fact that here mixing of potential vorticity is achieved not by the action of small coherent vortices, but instead occurs in (initially) narrow critical layer regions of the large-scale Rossby waves forced by the topography.

III. JET DEVELOPMENT

We begin by considering selected integrations at times for which the energy of the flow is the same in each case, in particular for which $L_{\mathrm{Rh}}/L_f = 3/4$ (see dotted line in Fig. 1). This can be compared with cases of Ref. 9 where $L_{\mathrm{Rh}}/L_f \gtrsim 8$ for the cases of point vortex forcing (Sec. 4.1 therein) or $L_{\mathrm{Rh}}/L_f \gtrsim 2$ for the cases of band-limited spectral space forcing (Sec. 4.3 therein). In Fig. 3, we show three representative cases $a_0 = 0.128$, $a_0 = 0.016$, and $a_0 = 0.002$, at times $t = 45$, 1760, and 117440, respectively, the times at which L_{Rh}/L_f first exceeds 3/4. The corresponding values of $L_{\mathrm{Rh}}/L_\varepsilon$ are approximately 2.0, 4.2, and 9.8. The structure of the potential vorticity varies in a way consistent with the results of Ref. 9. In the case $a_0 = 0.128$, for which $L_{\mathrm{Rh}}/L_\varepsilon \approx 2.0$, there is no evidence of any systematic organization of the potential vorticity into a zonally aligned distribution: mixing induced by the topographic forcing overwhelms the tendency of the flow to organize into any kind of staircase structure. At the other extreme, in the case $a_0 = 0.002$ ($L_{\mathrm{Rh}}/L_\varepsilon \approx 9.8$) the result of potential vorticity mixing is clearly visible, with distinct homogenization in certain regions separated by strong gradients. The intermediate case $a_0 = 0.016$ lies somewhere in between: mixing of potential vorticity is visible, as are the beginnings of the organization of the potential vorticity into a banded distribution, albeit a weakly differentiated one.

It is instructive to follow the evolution of the intermediate case $a_0 = 0.016$ to later times, for which both L_{Rh}/L_f and $L_{\mathrm{Rh}}/L_\varepsilon$ are larger. Figure 4 shows the potential vorticity for this case at times $t = 4000$, $t = 8000$, and $t = 16\,000$ and illustrates the emergence of the staircase structure as the parameter $L_{\mathrm{Rh}}/L_\varepsilon$ increases from 5.3, 6.0, and 7.3, respectively. The corresponding profiles of potential vorticity as a function of equivalent latitude, $q(y_e)$ are shown in Fig. 5(a), indicating the

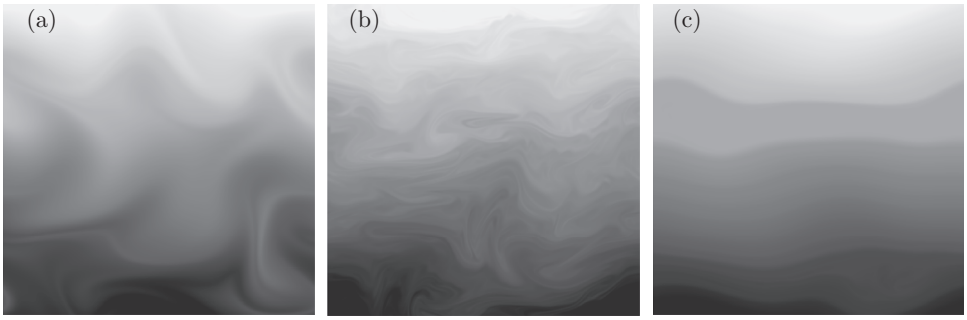

FIG. 3. $q(x, y)$ at the time for which L_{Rh}/L_f first exceeds 0.75; topographic forcing amplitudes $a_0 = 0.128$, 0.016, 0.002 (a–c); values of $L_{\mathrm{Rh}}/L_\varepsilon$ are 2.9, 4.2, and 9.8, respectively.

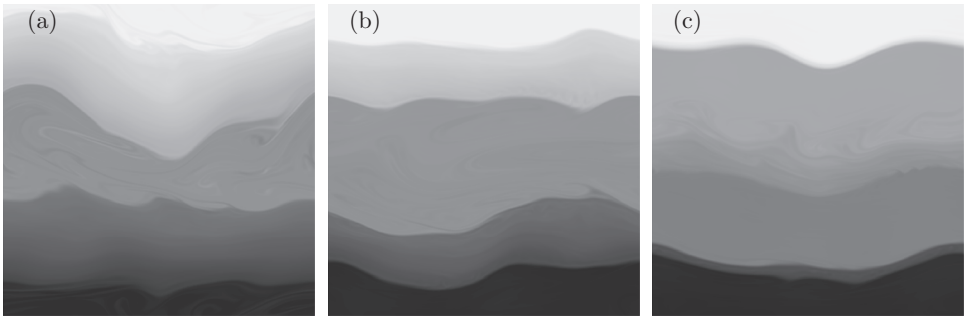

FIG. 4. $q(x, y)$ at $t = 4000$, $t = 8000$ and $t = 16\,000$ (a–c); topographic forcing amplitude $a_0 = 0.016$; values of $L_{\mathrm{Rh}}/L_\varepsilon$ are 5.3, 6.0, and 7.3, respectively.

extent to which the staircase profile is achieved. Note that in the equivalent latitude view, the sharp jumps in potential vorticity are well represented, despite the presence of large wave motions on the jets; in this case the simple zonal average $\bar{q}(y)$ (not shown) has a profile with considerably weaker latitudinal gradients. At the early time ($t = 4000$, dotted line in Fig. 5(a)) the potential vorticity is nearly perfectly mixed over two narrow latitudinal ranges near $y_e = 0$ and $y_e = \pm\pi$. At the intermediate time ($t = 8000$, thin continuous line), these mixed zones have increased in latitudinal extent, while elsewhere the potential vorticity profile remains close to that of the background βy (in sharp contrast to the case of small-scale forcing, where mixing is observed across the whole domain[9]). The increase is gradual and broadly consistent with a $t^{1/4}$ growth in latitudinal extent, expected from a purely zonally symmetric profile consisting of a single expanding mixed zone and linear increase in energy with time (see also the plot of $q(y_e, t) - \beta y_e$ shown in Fig. 8(d), below, and corresponding plots for cases with other forcing amplitudes).

The increase in the latitudinal extent of the mixed zones, as well as the absence of mixing in between, is a clear example of the way in which the background potential vorticity profile organizes mixing in such a way as to favour the development of the staircase profile. Within the mixing region, a downgradient potential vorticity flux implies a local deceleration, reducing the mean flow below its average value. As a result, the steep gradients at the edge of the mixed zone support Rossby edge waves whose westward relative phase propagation implies the existence of critical layers located within the mixed zone. Note that the relevant model of wave propagation here is that described by a free edge wave existing on a potential vorticity discontinuity, with westward phase speed relative to the jet lying between zero and the jet speed.[3] At $t = 8000$, for example, waves on the jump at

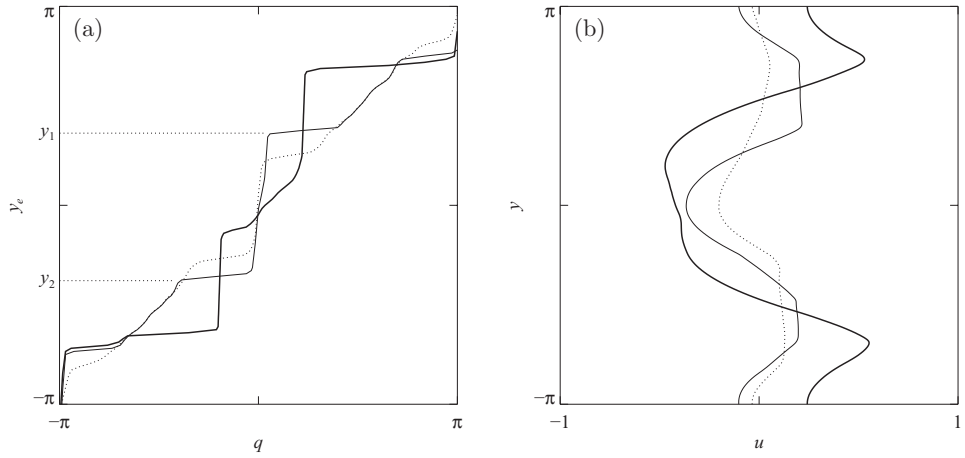

FIG. 5. (a) $q(y_e)$ and (b) $\bar{u}(y)$ from the fields shown in Fig. 4; times $t = 4000$ (dotted), $t = 8000$ (continuous), and $t = 16\,000$ (bold); topographic forcing amplitude $a_0 = 0.016$.

$y = y_1$ have a critical layer in the mixed zone below y_1, but no critical layer in the region immediately above y_1, where $q \approx \beta y_e$. This can be verified by reference to the corresponding profiles of zonal mean zonal velocity $\bar{u}(y)$ shown in Fig. 5(b), in which $\bar{u}$ decreases below y_1 but is approximately constant above. Nonlinear breaking of waves residing on the jump at y_1 into the critical layer region below will act to entrain fluid from the region above into the mixed zone. The situation is similar to the predominantly one-way wave breaking at the edge of the winter stratospheric polar vortex, in which polar air is entrained and mixed into the surf zone,[18,21,22] or on the subtropical tropopause.[23] A corresponding entrainment of the fluid from the region below the lower edge of the mixed zone at y_2 results in the growth of the extent of the mixed zone, while its average potential vorticity remains unchanged. Related behaviour was observed in a spherical shallow water model in which an initial critical layer in a pre-existing background flow exhibited a poleward migration in conjunction with the development of the mixed zone.[24]

At later times the simple growth of the mixed zone is further complicated by the fact that the critical layers below y_1 and above y_2 themselves have limited latitudinal extent depending on the amplitude and wavelength of the waves residing on each jump: the critical layer is located beneath y_1 at a distance roughly proportional to the inverse wavenumber of the waves residing on the jump, and, assuming wave slopes on the jump to be limited to $O(1)$, the width of the closed streamline region will also be limited by the inverse wavenumber. This means that when the width of the mixed zone exceeds a critical distance, determined by the inverse wavenumber which is here fixed, the upper and lower critical layers will cease to overlap and mixing between them will be suppressed. At this point the average potential vorticity of the upper critical layer will begin to increase, while that of the lower critical layer will decrease, due to the continued entrainment of high and low potential vorticity from above and below the respective layers. The result of this decoupling of the upper and lower critical layers is a splitting of the mixed zone, as can be seen to have occurred in the central zone in Fig. 5 (visible also in the time evolution of $q(y_e, t) - \beta y_e$ shown in Fig. 8(d)).

The value of L_{Rh}/L_f at the later time (Fig. 4(c)) is approximately 1.1; i.e., the forcing scale and the Rhines scale are practically the same. In fact from the observed jet structure alone, it is also clear that the energy containing scales at the final time are the same as the forcing scale. Here, L_f is defined simply as $L_f = k_f^{-1}$. If the jet scale L_j is defined similarly as $1/k_j$, where k_j is the dominant wavenumber of the jets, here 2, we obtain the ratio $L_j/L_f = 1$. In other words, jets, the dominant energy containing features of the flow, are created at scales the same as those of the forcing. Note that the dominant wavenumbers also undergo a fundamental change in structure as the mean flow develops, from isotropic waves with wavenumber magnitude $|\mathbf{k}| = k_f$ at early times, to the edge waves (evanescent in y) seen in, for example, Fig. 4. By either measure, the inverse energy cascade, in the usual sense of the term, appears not to be involved in the process of jet formation in the present case.[25]

The restriction of potential vorticity mixing to within critical layer regions is illustrated clearly in the weaker forcing case $a_0 = 0.004$. Figure 6 shows the potential vorticity field at times $t = 32\,000$, $t = 64\,000$, and $t = 160\,000$. The corresponding profiles $q(y_e)$ and $u(y)$ are shown in Fig. 7. At earlier time, potential vorticity is well mixed across four narrow regions (considerably

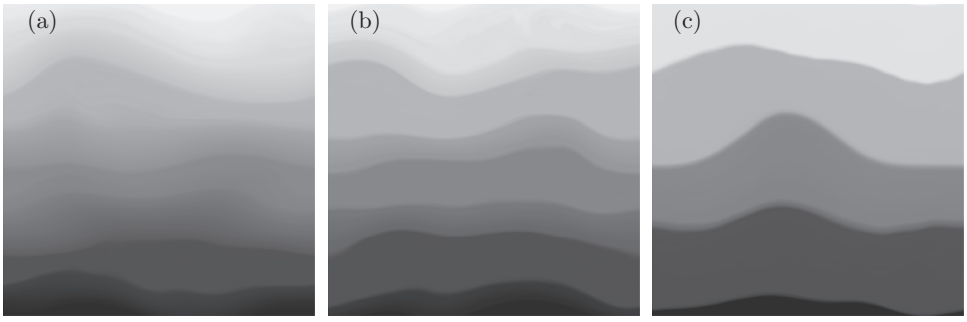

FIG. 6. q at $t = 32\,000$, $t = 64000$, and $t = 160\,000$ (a–c); topographic forcing amplitude $a_0 = 0.004$.

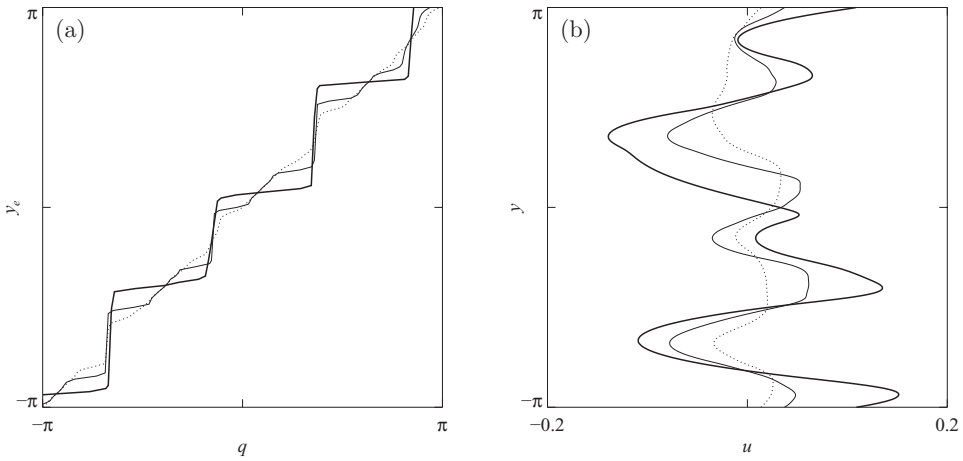

FIG. 7. (a) $q(y_e)$ and (b) $\bar{u}(y)$ at times $t = 32\,000$ (dotted), $t = 64\,000$ (continuous), and $t = 160\,000$ (bold); topographic forcing amplitude $a_0 = 0.004$.

narrower than the scale of the forcing), while elsewhere local values remain close to the background βy. In this case, the approximately equal initial spacing of the mixed zones leads to the formation of a regular staircase structure, at least in the potential vorticity field, although it is interesting to note that the small irregularities in the potential vorticity distribution result in quite marked irregularities in the zonal mean jet structure $\bar{u}(y)$. At the final time shown, the values of $L_{\mathrm{Rh}}/L_\varepsilon$ and L_{Rh}/L_f are 11.0 and 1.0, respectively, again illustrating the absence of inverse cascade in the jet formation process (or, in terms of the jet structure, the jet scale is here $L_j = 1/4$, giving $L_j/L_f = 1/2$).

Again, the main feature to note in Fig. 6 is the localized nature of the potential vorticity mixing at early times, and how the mixing regions grow in time with little change to the potential vorticity distribution between these regions. The growth of the mixing regions dominates all other changes to the mean flow. The critical layer regions may thus be regarded as local sinks of wave activity. Here, waves are generated randomly and homogeneously throughout the domain. Wave breaking, in contrast, is restricted to regions where the potential vorticity gradient is weaker than the background β; outside of these regions waves are linear and freely propagating. By the Taylor identity, the downgradient potential vorticity mixing within the critical layer is identical to an eddy momentum flux divergence, or a convergence of wave activity flux into the layer. The absence of wave breaking in the area between critical layers is evident in the time evolution of the potential vorticity anomaly, $q(y_e, t) - \beta y_e$, shown in Fig. 8, particularly those cases of weaker a_0. In the two weakest forcing cases, $a_0 = 0.001$ and $a_0 = 0.002$ (lower two panels), the potential vorticity in the regions outside the critical layers remains close to the background β for the entire length of the integration, all wave activity flux convergence being confined to the critical layers and contributing to their growth in time. Profiles of $q(y_e)$ for these two cases at $t = 320/a_0$ and $t = 640/a_0$, shown in Figs. 9(c) and 9(d), make clear that almost all mean flow changes are confined to the mixed regions. This evolution may be contrasted with the case of small-scale forcing, in which many jets typically emerge spontaneously throughout the domain and then merge into fewer jets as the total energy of the flow increases.

The general behaviour described above appears to be robust. In other integrations using the same physical parameters, but with different realizations of the random forcing, a variety of different late-time jet configurations were obtained, depending on the precise locations where potential vorticity first becomes mixed at early times. This initial seeding of the jets is presumably sensitive to the details of early wave transience and wave-wave interactions. Once the potential vorticity is mixed in a given region, however, in all cases observed the subsequent evolution consists of the preferential broadening of that particular region. The evolution is a good example of the idea that the resting planetary profile of potential vorticity may be considered as "an unstable equilibrium in the presence of Rossby waves and instabilities."[4]

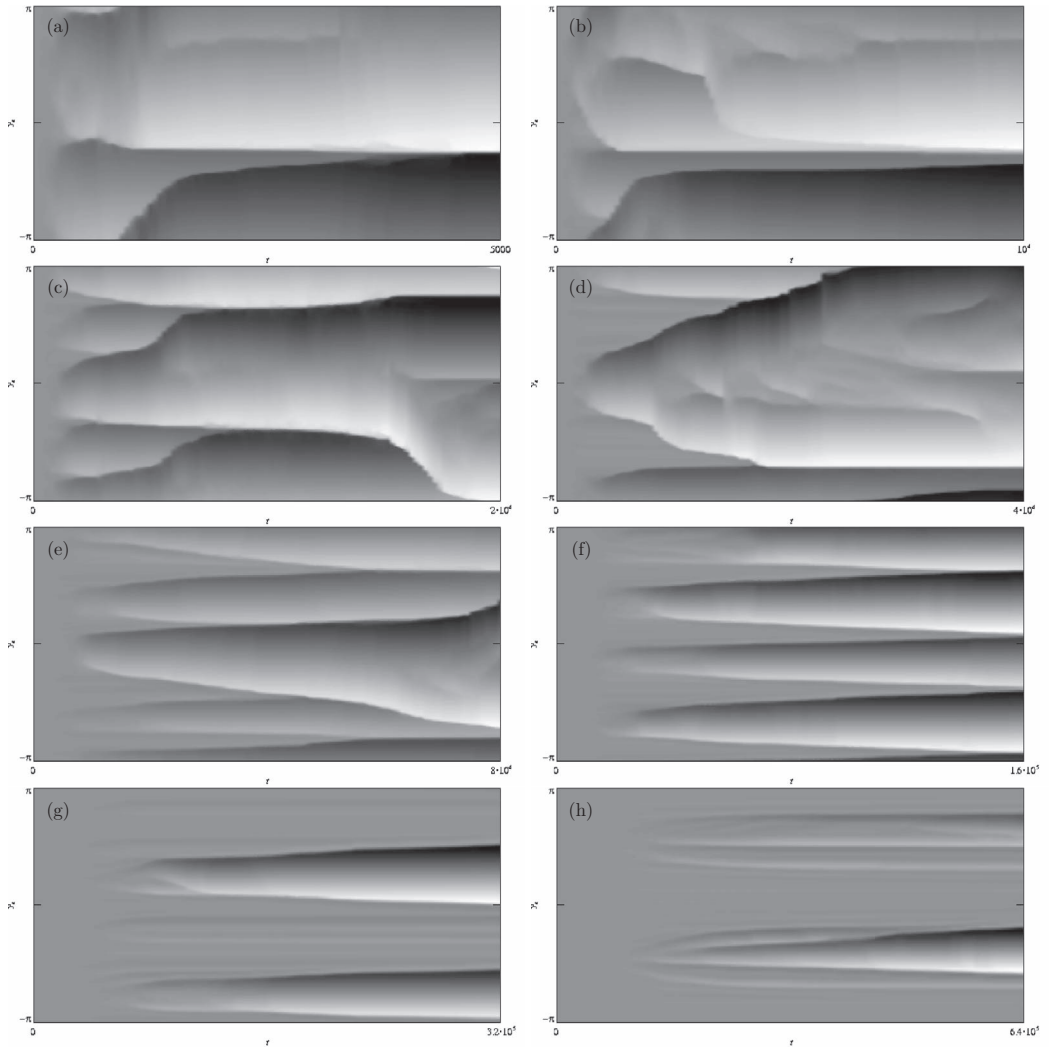

FIG. 8. Time evolution of equivalent latitude potential vorticity anomaly, $q(y_e, t) - \beta y_e$ for topographic forcing amplitudes $a_0 = 0.128$, 0.064, 0.032, 0.016, 0.008, 0.004, 0.002, and 0.001 (a–h).

In cases of stronger forcing, jet interactions become important when the mixed regions grow to an extent that they start to overlap, at which point one mixed region may continue to grow at the expense of another (for example, Figs. 8(c) and 8(d)). Splitting of a mixed region, as described above for the case $a_0 = 0.016$ is also apparent in the other strongly forced cases, e.g., $a_0 = 0.032$ or $a_0 = 0.064$. The profiles of $q(y_e)$ for the case $a_0 = 0.008$, shown in Fig. 9(b), provide a clear example

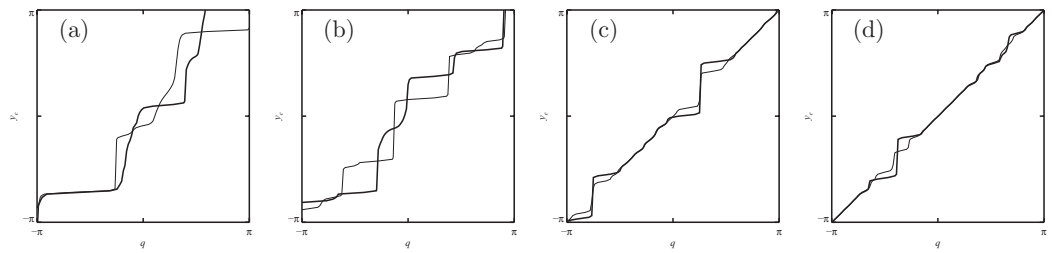

FIG. 9. $q(y_e)$ at the final time (bold) and half time (feint); topographic forcing amplitude $a_0 = 0.016$, 0.008, 0.002, 0.001 (a–d; for $a_0 = 0.004$ see Fig. 7(a)).

of the splitting of a mixed zone and the formation of a new stair step (just below $y_e = 0$; see also Fig. 8(e)). In the profile for the case $a_0 = 0.016$, Fig. 9(a), the final time jump just above $y_e = 0$ can be seen from Fig. 8(d) to also have emerged out of a mixed zone. In the very strongest forcing cases, however, the final energies are large enough that multiple jumps are not possible, the mixed regions saturate at the domain scale and the final states consist of two regions of uniform potential vorticity separated by a single jump.

IV. CHARACTERIZATION OF MIXING

The time of onset of the development into a staircase distribution may be defined as the time at which the mean potential vorticity gradient first decreases below a critical value. The first occurrence in each integration of mixed regions in which $dq/dy_e < 0.1$ is indicated in Fig. 1 by the cross marks. For the strong forcing cases, with a_0 between 0.128 and 0.016, the onset of the mixing regions occurs approximately at a time proportional to the enstrophy-based time scale $T_\eta = (k_f^2\varepsilon)^{-1/3}$ discussed in Sec. II. For the weak forcing cases, $a_0 = 0.008$ and below, on the other hand, the first onset of the mixing regions occurs considerably later. The difference in onset times points to a fundamental difference between the mixing present in fully turbulent flows and that taking place in flows that are dominated by linear wave motions except in isolated critical layer regions. The difference may be characterized by the relative importance at the forcing scale k_f of the terms $J(\psi, \zeta)$ and $\beta\psi_x$ comprising the advective term $J(\psi, q)$ in (1). To estimate the size of these terms we can use (8) with $\varepsilon = \dot{\mathcal{E}}$ to give $\varepsilon \sim k_f^{-2}a_0^2\tau_f^{-1}$, where we are assuming that $\psi \sim k_f^{-2}q_{\text{topo}} \sim k_f^{-2}a_0$ for motions near the forcing scale. Using $\tau_f \sim k_f/\beta$ as described in Sec. II gives $\varepsilon \sim k_f^{-3}a_0^2\beta$. Replacing all spatial derivatives with k_f (appropriate for dominant motions near the forcing scale) and eliminating a_0 then gives the relative magnitude of the terms $J(\psi, \zeta)$ and $\beta\psi_x$ as

$$J(\psi, \zeta)/\beta\psi_x \sim (\varepsilon k_f^5/\beta^3)^{1/2} \sim (L_\varepsilon/L_f)^{5/2}. \tag{9}$$

When L_ε/L_f is large, the nonlinear term dominates over the linear $\beta\psi_x$ and motions are turbulent rather than wave-like, as characterized by Fig. 3(a). When it is small, $\beta\psi_x$ dominates and motions are wave-like; mixing is absent except in critical layer regions where nonlinearity again becomes important. Based on the above integrations, the numerical value of L_ε/L_f separating these two regimes appears to be in the region of 1/6, $L_\varepsilon/L_f = 1/6$ corresponding in Fig. 1 to the line with slope 1/6 approximately separating the two sets of integrations $a_0 \geq 0.016$ and $a_0 \leq 0.008$. The integrations reported in Ref. 9 with band-limited forcing (lying just above the dashed line in Fig. 1) all have $L_\varepsilon/L_f > 1/6$, while those with broad-band forcing have still larger values, and thus, the mixing in that paper is predominantly by turbulent eddies rather than in Rossby wave critical layers. Note, for further comparison that the values of L_ε/L_f used in the low-wavenumber forcing experiments of Maltrud and Vallis[11] are significantly larger. A direct comparison is not possible because the frictional damping term used in Ref. 11 was restricted to the lowest wavenumbers, complicating the relation between L_{Rh} and L_ε. Approximate values, however, are $L_f \approx 1/12$ and L_ε between about 0.2 and 1, giving L_ε/L_f between about 2.4 and 12; as evident from Figures 1(b)–1(d) in Ref. 11, mixing is dominated by a strongly nonlinear turbulent flow.

For $L_\varepsilon/L_f < 1/6$ (cases $a_0 \leq 0.008$), the onset of critical layer mixing appears to develop as soon as the ratio L_{Rh}/L_f exceeds a value of about 3/4. Note that this point should be interpreted as only the beginning of the development of the potential vorticity into a staircase distribution. As is clear from Fig. 9, the full staircase takes much longer to develop, particularly at the lowest forcing amplitudes. However, the results suggest that the condition $L_{\text{Rh}}/L_\varepsilon \gtrsim 6$ obtained in Ref. 9 as necessary for staircase formation should be supplemented with the additional one of $L_{\text{Rh}}/L_f \gtrsim 1$, in cases when the mixing responsible for the staircase development is critical layer dominated, that is when the ratio $L_\varepsilon/L_f \lesssim 1/6$. A combined condition for the staircase formation is thus $L_{\text{Rh}}/L_\varepsilon \gtrsim \max\{6, L_f/L_\varepsilon\}$.

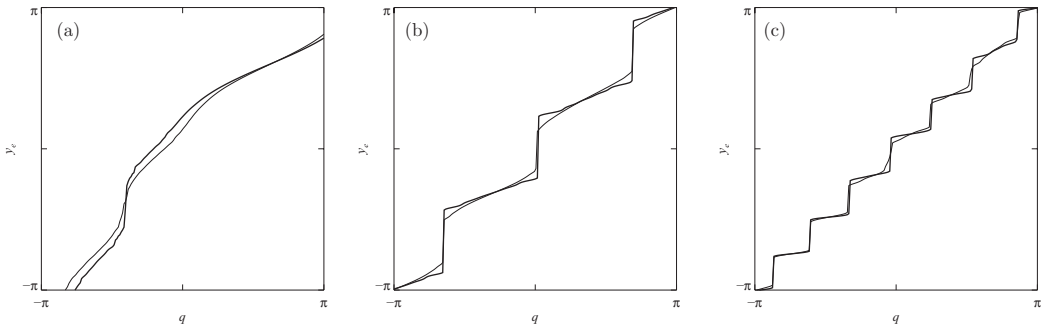

FIG. 10. $q(y_e)$ for the cases $L_\varepsilon/L_f = 1/6$ and $L_f = 1/2$, 1/4, 1/8 (a–c) at times such that $L_{\mathrm{Rh}}/L_\varepsilon = 7.5$ (light) and $L_{\mathrm{Rh}}/L_\varepsilon = 9.0$ (bold), equivalently $L_{\mathrm{Rh}}/L_f = 1.25$ and $L_{\mathrm{Rh}}/L_f = 1.5$.

V. VORTICITY FORCING

For comparison, we close with a brief examination of the case in which the flow is forced by a source term F in the vorticity equation, as in (3). This type of forcing is commonly used in studies of two-dimensional turbulence, whether isotropic or on the β-plane. It has the immediate advantage that the energy input rate may be specified *a priori*, for example, by assuming a Markovian time dependence for each Fourier component $\hat{f}_{\mathbf{k}}$ of F. As before, we first define

$$\tilde{f}_{\mathbf{k}}^{(n)} = \alpha \tilde{f}_{\mathbf{k}}^{(n-1)} + \sqrt{1-\alpha^2}\sigma_{\mathbf{k}}, \tag{10}$$

where $\sigma_{\mathbf{k}}$ is a random variable of zero mean, uniformly distributed on $[-1, 1]$, and now define

$$\hat{f}_{\mathbf{k}}^{(n)} = \frac{\varepsilon \tilde{f}_{\mathbf{k}}^{(n)}}{\langle \hat{\psi}_{\mathbf{k}}^{(n)} \tilde{f}_{\mathbf{k}}^{*(n)} \rangle} \tag{11}$$

ensuring that the rate of energy increase $\dot{\mathcal{E}} = \langle \hat{\psi}_{\mathbf{k}}^{(n)} \hat{f}_{\mathbf{k}}^{*(n)} \rangle$ is exactly ε. As before, the parameter α is related to the decorrelation time τ_f via $\alpha = 1 - \Delta t/\tau_f$, with τ_f again set to $5/\beta$.

While this method of forcing has the advantage that $\dot{\mathcal{E}}$ may be specified exactly, the loss of material conservation of potential vorticity may, however, be important in certain cases, depending on the relative sizes of the terms $J(\psi, q)$ and F in (3). If the nonlinear component $J(\psi, \zeta)$ is large relative to F, we may expect non-conservative effects of the forcing to be unimportant. In the regime of interest here, however, the response of the flow to the weak, large-scale forcing is largely that of linear wave propagation, $J(\psi, \zeta)$ is small except in critical layers, and the main balance in (3) is between q_t and $\beta\psi_x$, that is, linear wave motions, which, in the time average, induce no change to the mean flow. On the flanks of critical layers, where some entrainment and mixing occurs but where nonlinearity is still weak, the non-conservative and random effect of F may act to obscure the systematic steepening of potential vorticity gradients. Deeper within the critical layers, nonlinear mixing is dominant and the effects of non-conservative F are negligible.

This interpretation is borne out by numerical integrations of (3) in which the Fourier components of F are Markovian processes as described above, while now the spectrum of $\tilde{f}_{\mathbf{k}}$ is $= 1$ for $k \in [k_f - \delta_k, k_f + \delta_k]$ and $= 0$ otherwise. A large number of integrations were performed, with a range of values of both ε and k_f, or equivalently of L_ε and L_f. The region of parameter space covered by the integrations corresponds closely to that shown in Fig. 1, the main difference now being that the evolution follows perfectly straight lines through the origin with slope L_ε/L_f. Values of ε and k_f were chosen such that $L_\varepsilon/L_f = 1$, 1/2, 1/4, 1/6, and 1/8, and for each of these three integrations were performed with $k_f = L_f^{-1} = 2$, 4, 8. Plotting the point at which dq/dy_e first decreased below a value of 0.1 gave a pattern qualitatively similar to the crosses in Fig. 1 (not shown), the onset of the mixing regions appearing later than predicted by T_η for all cases with small L_ε/L_f.

The non-conservative effects of the forcing, however, obscured a more detailed investigation at smaller L_ε/L_f. In Fig. 10 we show the late time profiles $q(y_e)$ for three cases with $L_\varepsilon/L_f = 1/6$, with $k_f = L_f^{-1} = 2$, 4, 8. The closest comparison is between the left hand panel of Fig. 9 and the left hand

panel of Fig. 10, for which the values of L_{Rh}, L_ε, and L_f at the final time (bold) are similar. The main point is that while mixing of potential vorticity is complete in distinct regions, as before, between these regions the tendency towards gradient intensification is obscured by the non-conservative effect of the forcing, which is continuously blurring the jumps between critical layer regions. It is of interest to note that the smoothing effect appears less pronounced when the forcing is concentrated at smaller scales (as was the case in Ref. 9), at least for the range of forcing amplitudes considered here, even though the parameter L_ε/L_f is here the same between cases, possibly an indication that finite domain effects are present in the case $k_f = 2$. However, even at larger k_f, gradients between mixed zones are in general less than in the cases with topographic forcing. The effect becomes increasingly pronounced at smaller values of L_ε/L_f: when $L_\varepsilon/L_f = 1/8$ (not shown) the profiles of $q(y_e)$ are blurred to the extent that the staircase profile is not well realised at any $k_f \leq 8$.

VI. CONCLUSIONS

Although the arrest of the inverse energy cascade by Rossby wave generation is commonly cited as the mechanism responsible for the formation of zonal jets in planetary atmospheres and oceans, the direct diagnostic relation between potential vorticity and streamfunction means that jets will robustly arise from *any* mixing of the background resting planetary vorticity into a distribution that consists of latitudinally distinct regions of enhanced and reduced potential vorticity gradient. In general, there is no reason why the mixing process needs to act predominantly at scales smaller than the jet or Rhines scale. In contrast, in this paper, we have demonstrated explicitly that potential vorticity mixing by large-scale waves generated by time-varying bottom topography can robustly lead to zonal jets with an associated potential vorticity distribution which is close to that of the ideal staircase, comprising a piecewise constant profile, monotonic in latitude. In the experiments reported here, jet formation is thus independent of any notion of an inverse energy cascade in the traditional sense, which by construction is absent. The idea of jet formation, or at least jet sharpening, by purely large-scale wave breaking processes is in accordance with the well-known behaviour of the winter polar stratosphere, where large-scale wave breaking mixes potential vorticity in a surf zone and steepens the gradients at the polar vortex edge. Our results demonstrate that similar behaviour is possible even in the more general situation in which there is no preexisting background shear and associated critical layer; in other words, the mixing and critical layer may arise spontaneously from a resting state.

Given the widespread appeal to the inverse cascade in the literature on zonal jets, our explicit demonstration of jet formation using large-scale forcing should serve as a useful illustration of the more general nature of mixing-induced jets. Perhaps more importantly, however, the present study highlights an important distinction between the character of potential vorticity mixing depending on whether the system is forced at small or at large scales. An important parameter controlling the degree of nonlinearity in the flow response to the forcing is L_ε/L_f, which can be obtained from a simple scale analysis of the equations of motion. The numerical results presented here suggest that when $L_\varepsilon/L_f \gtrsim 1/6$ potential vorticity mixing occurs by fully nonlinear turbulent advection, whereas when $L_\varepsilon/L_f \lesssim 1/6$ it occurs predominantly in latitudinally confined Rossby wave critical layers. These critical layers separate regions in which the flow dynamics is dominated by linear wave propagation, and in which the mean potential vorticity profile remains close to that of the background planetary profile.

In the continually-forced, time-evolving situation considered here, in which the energy is on average increasing steadily, the critical layers expand in time by entraining fluid from the background, linear wave regions, until they occupy the whole domain. Breaking of waves on the edges of the mixed regions is predominantly one way, into the mixed region, similar to the breaking waves on the edge of the stratospheric polar vortex. The critical layers act as a sink of wave activity in the sense that the divergence of wave activity flux, equal to the eddy potential vorticity flux, is dominant in the mixed regions, as can be seen immediately from the fact that changes to the mean potential vorticity profile are restricted to the mixed regions, with little change in the background profile during their growth. Where critical layers initially form varies randomly among different realizations of the forcing, and presumably depends on details of wave transience during the early evolution. Once

formed they tend to grow *in situ* until either (i) the mixed zone becomes so wide that the critical layers of waves on either flank become disconnected, with the result that entrained fluid is no longer mixed across the whole region, resulting in the birth of a new jet in the centre of the mixed region; or (ii) two mixed regions encroach on one another, with one continuing to grow at the expense of the other.

The present results provide an additional condition for the formation of strong jets. In Ref. 9 it was demonstrated that in the case in which the forcing is located at scales significantly smaller than the Rhines scale, the condition $L_{\mathrm{Rh}}/L_\varepsilon \gtrsim 6$ is required for the emergence of strong jets, with the staircase limit being approached for values somewhat higher, $L_{\mathrm{Rh}}/L_\varepsilon \sim O(10)$. The present results suggest that this condition be supplemented with the additional one of $L_{\mathrm{Rh}}/L_f \gtrsim 1$ in cases where the forcing is such that $L_\varepsilon/L_f \lesssim 1/6$, with staircase formation occurring for $L_{\mathrm{Rh}}/L_\varepsilon \gtrsim \max\{6, L_f/L_\varepsilon\}$. In other words there is an upper limit to the scale of the forcing relative to L_{Rh} for which critical layer mixing occurs. As an aside we note that the approach used in the present paper, in which the removal of energy by frictional processes is absent, supports the interpretation of Ref. 9 of the physical effect of forcing strength on the jet formation, namely, that what controls the sharpness of the staircase is the intensity of the mixing generated by the forcing, rather than any effect related to the frictional damping.

Finally, we note that in the problem in which the forcing is at large scales and has a weak rate of energy input, care must be taken in the way the forcing is implemented. With simple additive forcing, represented by a source term in the vorticity equation, such as is commonly used in idealized studies of two-dimensional turbulence, the loss of material conservation of potential vorticity may obscure the formation of strong latitudinal gradients. Forcing with a time-varying bottom topography avoids this issue since material conservation of potential vorticity is preserved, allowing the systematic effect of weak potential vorticity mixing over very long times to be captured accurately. In the situation of the atmosphere, the system may be considered as a simple representation of the effect of upward propagation of Rossby waves from a dynamically active layer into the layer of interest. More generally, the forcing may be considered simply as a physical means of wave excitation in the layer of interest in a dynamically realistic way.

ACKNOWLEDGMENTS

The authors wish to thank Michael McIntyre and Peter Rhines for helpful comments and discussions. This work was supported by the National Science Foundation through Grant No. ATM-0827210.

[1] G. I. Taylor, "Eddy motion in the atmosphere," Philos. Trans. R. Soc. London A **215**, 1–26 (1915).
[2] F. P. Bretherton, "Critical layer instability in baroclinic flows," Q. J. R. Meteorol. Soc. **92**, 325–334 (1966).
[3] M. E. McIntyre, "Potential-vorticity inversion and the wave–turbulence jigsaw: some recent clarifications," Adv. Geophys. **15**, 47–56 (2008).
[4] T. J. Dunkerton and R. K. Scott, "A barotropic model of the angular momentum conserving potential vorticity staircase in spherical geometry," J. Atmos. Sci. **65**, 1105–1136 (2008).
[5] J. G. Esler, "The turbulent equilibration of an unstable baroclinic jet," J. Fluid Mech. **599**, 241–268 (2008).
[6] A. F. Thompson and W. R. Young, "Two-layer baroclinic eddy heat fluxes: zonal flows and energy balance," J. Atmos. Sci. **64**, 3214–3231 (2007).
[7] P. B. Rhines, "Waves and turbulence on a beta-plane," J. Fluid Mech. **69**, 417–443 (1975).
[8] G. P. Williams, "Planetary circulations: 1. Barotropic representation of Jovian and terrestrial turbulence," J. Atmos. Sci. **35**, 1399–1424 (1978).
[9] R. K. Scott and D. G. Dritschel, "The structure of zonal jets in geostrophic turbulence," J. Fluid Mech. **711**, 576–598 (2012).
[10] D. G. Dritschel and M. E. McIntyre, "Multiple jets as PV staircases: the Phillips effect and the resilience of eddy-transport barriers," J. Atmos. Sci. **65**, 855–874 (2008).
[11] M. E. Maltrud and G. K. Vallis, "Energy spectra and coherent structures in forced two-dimensional and beta-plane turbulence," J. Fluid Mech. **228**, 321–342 (1991).
[12] G. K. Vallis, *Atmospheric and Oceanic Fluid Dynamics* (Cambridge University Press, Cambridge, England, 2006), p. 745.
[13] S. Sukoriansky, N. Dikovskaya, and B. Galperin, "On the arrest of inverse energy cascade and the Rhines scale," J. Atmos. Sci. **64**, 3312–3327 (2007).
[14] H.-P. Huang and W. A. Robinson, "Two-dimensional turbulence and persistent zonal jets in a global barotropic model," J. Atmos. Sci. **55**, 611–632 (1998).

[15] S. Danilov and D. Gurarie, "Scaling, spectra and zonal jets in beta-plane turbulence," Phys. Fluids **16**, 2592–2603 (2004).
[16] R. K. Scott and L. M. Polvani, "Forced-dissipative shallow water turbulence on the sphere and the atmospheric circulation of the gas planets," J. Atmos. Sci. **64**, 3158–3176 (2007).
[17] M. E. McIntyre, "How well do we understand the dynamics of stratospheric warmings?" J. Meteorol. Soc. Jpn. **60**, 37–65 (1982), special issue in commemoration of the centennial of the Meteorological Society of Japan, edited by K. Ninomiya.
[18] M. N. Juckes and M. E. McIntyre, "A high resolution, one-layer model of breaking planetary waves in the stratosphere," Nature **328**, 590–596 (1987).
[19] L. M. Polvani, D. W. Waugh, and R. A. Plumb, "On the subtropical edge of the stratospheric surf zone," J. Atmos. Sci. **52**, 1288–1309 (1995).
[20] T. Y. Hou and R. Li, "Dynamic depletion of vortex stretching and non-blowup of the 3-D incompressible Euler equations," J. Nonlinear Sci. **16**, 639–664 (2006).
[21] W. A. Norton, "Breaking Rossby waves in a model stratosphere diagnosed by a vortex-following coordinate system and a technique for advecting material contours," J. Atmos. Sci. **51**, 654–673 (1994).
[22] D. W. Waugh and R. A. Plumb, "Contour advection with surgery: a technique for investigating finescale structure in tracer transport," J. Atmos. Sci. **51**, 530–540 (1994).
[23] R. K. Scott and J.-P. Cammas, "Wave breaking and mixing at the subtropical tropopause," J. Atmos. Sci. **59**, 2347–2361 (2002).
[24] P. B. Rhines, "Jets and orography: Idealized experiments with tip jets and Lighthill blocking," J. Atmos. Sci. **64**, 3627–3639 (2007).
[25] In terms of the two-dimensional energy spectrum, a transfer of energy to the lowest zonal wavenumber has of course been achieved, though this is simply the manifestation of the zonal jet formation, rather than an inverse energy cascade in the usual sense.